NUCLEAR THEORY, Vol. 29 (2010)
eds. A. Georgieva, N. Minkov, Heron Press, Sofia

Pygmy Resonances in Exotic Nuclei

N. Tsoneva[1], **H. Lenske**[1]

[1] Institut für Theoretische Physik, Universität Giessen, Heinrich-Buff-Ring 16, 35390 Giessen, Germany

Abstract. Theoretical approach is applied for investigation of dipole and other multipole excitations in skin nuclei, particular exploring their connection to the thickness of the neutron or proton skin. The method relies on density functional theory which provides a proper link between nuclear many-body theory of the nuclear ground state and its phenomenological description. The nuclear excited states are calculated within the Quasiparticle-Phonon Model including up to three-phonon structures. Low-energy dipole and quadrupole excitations are explained as pygmy dipole and pygmy quadrupole resonances, respectively.

1 Introduction

The development of experimental facilities on radioactive nuclear beams reveals the opportunity to investigate unknown regions of exotic nuclei, far from the valley of β-stability. The observation of halos in light nuclei [1] followed by the skin phenomena in medium and heavy nuclei [2, 3] gives new insight into the isospin dynamics of nuclear matter. One of the most interesting findings, was the observation of enhanced dipole strength close to the particle emission threshold as a common feature of stable and unstable nuclei with neutron excess [4–8]. It was associated with oscillations of a small portion of neutron-rich nuclear matter relative to the rest of the nucleus. As this clustering of strong dipole transitions resembles a resonance it was named pygmy dipole resonance (PDR).

Here, we present systematic theoretical studies, based on method incorporating self-consistent Skyrme Hartree-Fock-Bogolubov (HFB) [9] and Quasiparticle-Phonon Model (QPM) theory [10], of dipole and other multipole excitations over isotonic and isotopic chains of nuclei with predominantly neutron excess [7, 8, 11–15]. Our calculations indicate a correlation between the observed total PDR strength and the neutron-to-proton ratio N/Z [13]. From the analysis of transition densities, the unique behavior of the PDR is revealed, making it distinct from giant dipole resonance (GDR). In addition, it has been suggested that the PDR is independent of the type of nucleon excess (neutron or proton) [13].

Recent investigations of low-energy E1 and spin-flip M1 excitations in $N = 82$ nuclei [14] allow to decompose the dipole strength below the GDR to elastic E1 component, related to skin oscillations and PDR, and background component composed of elastic and inelastic E1 and M1 transitions, respectively. The obtained information reveals new aspects in the isospin dynamics of the nucleus.

An obvious question, coming up immediately in this connection, is to what extent the presence of a neutron or proton skin will affect excitations of other multipolarities and *vice versa*. Promising candidates are low-energy 2^+ states, especially those in excess of the spectral distributions known from stable nuclei. Quadrupole response functions are investigated theoretically in neutron-rich Sn nuclei. A close connection of low-energy 2^+ excitations and nuclear skins is discussed. These quadrupole states are related to Pygmy Quadrupole Resonance (PQR) [15, 16].

2 Theoretical Approach

The model Hamiltonian resembles in structure the traditional QPM model [10] but in detail differs in the physical content in important aspects as discussed in Ref. [11, 13]. In this sense, the approach is able to describe the nuclear ground state properties like binding energies, neutron and proton root mean square radii and the difference between them defining the nuclear skin, and separation energies [13]. The model Hamiltonian is given by:

$$H = H_{MF} + H_M^{ph} + H_{SM}^{ph} + H_M^{pp} \quad . \tag{1}$$

Here, $H_{MF} = H_{sp} + H_{pair}$ is the mean-field part. Different from the standard QPM scheme this part is obtained from self-consistent HFB theory [9]. The H_{MF} defines the single particle properties including potentials and pairing interactions for protons and neutrons, such that also dynamical effects beyond mean-field can be taken into account. That goal is achieved in practice by using fully microscopic HFB potentials and pairing fields as input but performing a second step variation with scaled auxiliary potentials and pairing fields readjusted in a self-consistent manner such that nuclear binding energies and other ground state properties of relevance are closely reproduced.

H_M^{ph}, H_{SM}^{ph} and H_M^{pp} are residual interactions, taken as a sum of isoscalar and isovector separable multipole and spin-multipole interactions in the particle-hole and multipole pairing interaction in the particle-particle channels. The multiple-multipole coupling constants of the residual interaction are fitted to the energies and transition rates of low-lying collective excitations and giant resonances [17].

2.1 Nuclear Ground State

The reliable description of ground state properties is of genuine importance for extrapolations of QRPA and QPM calculations into unknown mass regions. Taking advantage of the Kohn-Sham theorem [18, 19] of Density Functional Theory (DFT) the total binding energy $B(A)$ of the nucleus could be expressed as an integral over an energy density functional with (quantal) kinetic (τ) and self-energy parts, respectively,

$$B(A) = \int d^3r \left(\tau(\rho) + \frac{1}{2}\rho U(\rho) \right) + E_{pair} \tag{2}$$

$$= \sum_j v_j^2 \left(e_j - < \Sigma >_j + \frac{1}{2} < U >_j \right) + E_{pair} \quad ,$$

and pairing contributions are indicated by E_{pair}. The second relation is obtained from Hartree-Fock-Bogoliubov (HFB) theory with occupancies v_j^2 and potential energies $< U >_j$ of the occupied levels j, see e.g. [9]. Above, $U(\rho)$ is the proper self-energy, i.e. not including the rearrangement contributions from the intrinsic density dependence of nuclear interactions [9]. Hence, $U(\rho)$ has to be distinguished from the effective self-energy obtained by variation

$$\Sigma(\rho) = \frac{1}{2} \frac{\partial \rho U(\rho)}{\partial \rho} \tag{3}$$

and appearing in the single particle Schroedinger equation. In order to keep the QPM calculations feasible we choose $\Sigma \equiv U_{WS}$ to be of Wood-Saxon (WS) shape with adjustable parameters. By inversion and observing that the densities and potentials in a finite nucleus are naturally given parametrically as functions of the radius r, we find

$$\rho(r) U(r) = -2 \int_r^\infty ds \frac{\partial \rho(s)}{\partial s} U_{WS}(s) \quad . \tag{4}$$

Evaluating these relations with the microscopic proton and neutron densities obtained by solving the Schroedinger equation with U_{WS} the potential $U(\rho)$ is the self-consistently derived reduced self-energy entering e.g. into the binding energy.

In practice, for a given nucleus of mass A the depth of the central and spin-orbit potentials, radius and diffusivity parameters of U_{WS} are adjusted separately for protons and neutrons to the corresponding single particle separation energies, the total binding energy [20], the charge radii and (relative) differences of proton and neutron root-mean-square (RMS) radii,

$$\delta r = \sqrt{< r^2 >_n} - \sqrt{< r^2 >_p} \quad , \tag{5}$$

from our previous HFB calculations [9]. In ref. [13] theoretically obtained RMS radii are compared to those determined from charge exchange reactions for a number of Sn isotopes. The approach sketched above leads to very satisfactory results on binding energies and proton-neutron RMS-differences as shown in [11, 13]. A smooth dependence of the parameters on A is found which supports the reliability of the method.

Calculations of ground state neutron and proton densities for Z=50 and $N = 50$, 82 nuclei are shown in Figure 1. Of special importance for these investigations are the nuclear surface regions, where the formation of a skin takes place. A common observation found in the investigated isotopic and isotonic chains of nuclei is that the thickness of the neutron skin is related to the neutron-to-proton ratio N/Z. For example, in Sn isotopes with A$\geq$106 the neutron distributions

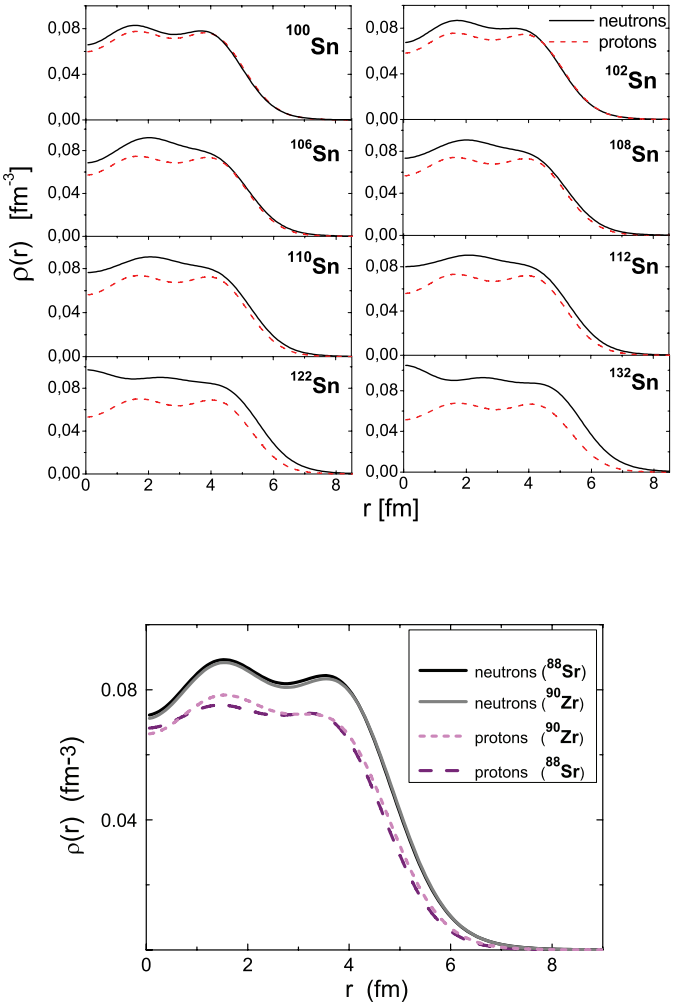

Figure 1. BCS ground state densities of Sn isotopes (upper panel) and $N = 50$, 82 isotones (lower panel) obtained by the phenomenological DFT approach and used in the QPM calculations.

begin to extend beyond the proton density and the effect continues to increase with the neutron excess, up to ^{132}Sn. Thus, these nuclei have a neutron skin. The situation reverses in $^{100-102}Sn$, where a tiny proton skin appears.

2.2 Nuclear Excited States

The nuclear excitations are expressed in terms of quasiparticle-random-phase-approximation (QRPA) phonons:

$$Q^{+}_{\lambda\mu i} = \frac{1}{2}\sum_{jj'}\Big(\psi^{\lambda i}_{jj'}A^{+}_{\lambda\mu}(jj') - \varphi^{\lambda i}_{jj'}\widetilde{A}_{\lambda\mu}(jj')\Big), \tag{6}$$

where $j \equiv (nljm\tau)$ is a single-particle proton or neutron state; $A^{+}_{\lambda\mu}$ and $\widetilde{A}_{\lambda\mu}$ are time-forward and time-backward operators, coupling two-quasiparticle creation or annihilation operators to a total angular momentum λ with projection μ by means of the Clebsch-Gordan coefficients $C^{\lambda\mu}_{jmj'm'} = \langle jmj'm'|\lambda\mu\rangle$. The excitation energies of the phonons and the time-forward and time-backward amplitudes $\psi^{\lambda i}_{j_1j_2}$ and $\varphi^{\lambda i}_{j_1j_2}$ in Eq. (6) are determined by solving QRPA equations [10].

Furthermore, the QPM provides a microscopic approach to multiconfiguration mixing [10]. The wave function of an excited state consists of one-, two- and three-phonon configurations [21]:

$$\Psi_\nu(JM) = \Bigg\{\sum_i R_i(J\nu)Q^{+}_{JMi} + \sum_{\substack{\lambda_1 i_1\\ \lambda_2 i_2}} P^{\lambda_1 i_1}_{\lambda_2 i_2}(J\nu)\Big[Q^{+}_{\lambda_1\mu_1 i_1}\times Q^{+}_{\lambda_2\mu_2 i_2}\Big]_{JM}$$

$$+ \sum_{\substack{\lambda_1 i_1 \lambda_2 i_2\\ \lambda_3 i_3 I}} T^{\lambda_1 i_1 \lambda_2 i_2 I}_{\lambda_3 i_3}(J\nu)\Big[\Big[Q^{+}_{\lambda_1\mu_1 i_1}\otimes Q^{+}_{\lambda_2\mu_2 i_2}\Big]_{IK}\otimes Q^{+}_{\lambda_3\mu_3 i_3}\Big]_{JM}\Bigg\}\Psi_0 \tag{7}$$

where R, P and T are unknown amplitudes, and ν labels the number of the excited states.

The electromagnetic transitions are described by transition operators accounting for the internal fermionic structure of the phonons [22]. The method allows for sufficiently large configuration spaces such that a unified description of low-energy single and multiple phonon states and the GDR is feasible. Such a unified treatment is exactly what is required in order to separate the multiphonon and the genuine PDR 1^- strengths in a meaningful way.

3 Discussion

From QRPA calculations in $^{110-132}$Sn, a sequence of low-lying one-phonon 1^- states of almost pure neutron structure at excitation energies $E^* = 6 - 7.5$ MeV is observed. These states correspond to excitations of least bound neutrons from the 3s-, 2p- and 2d-subshells and only a minor proton contribution less than 1%. Similar results are found also in $N = 50$, 82 isotones [7, 8]. These low-energy dipole states have been related to neutron PDR.

In the lightest $^{100-104}$Sn isotopes, the lowest dipole excitations at E*= 8.1-8.3 MeV are dominated by proton excitations involving quasibound $2p_{3/2}$ and

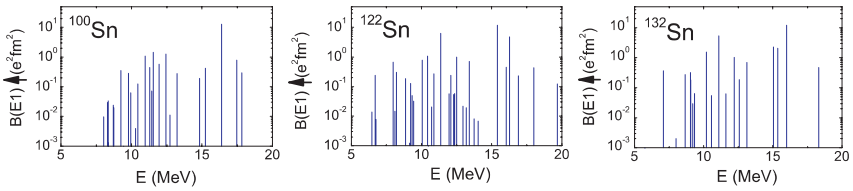

Figure 2. QRPA calculations of electric dipole strength distributions in Sn isotopes.

$1g_{9/2}$ proton states [13]. Electromagnetic breaking of isospin symmetry is the main reason for the persisting of low-energy dipole strength close to ^{100}Sn. QRPA calculations of dipole response functions in several tin isotopes are presented in Figure 2. The observed sequence of low-energy neutron or proton dipole states have been related to neutron or proton PDR, respectively [13].

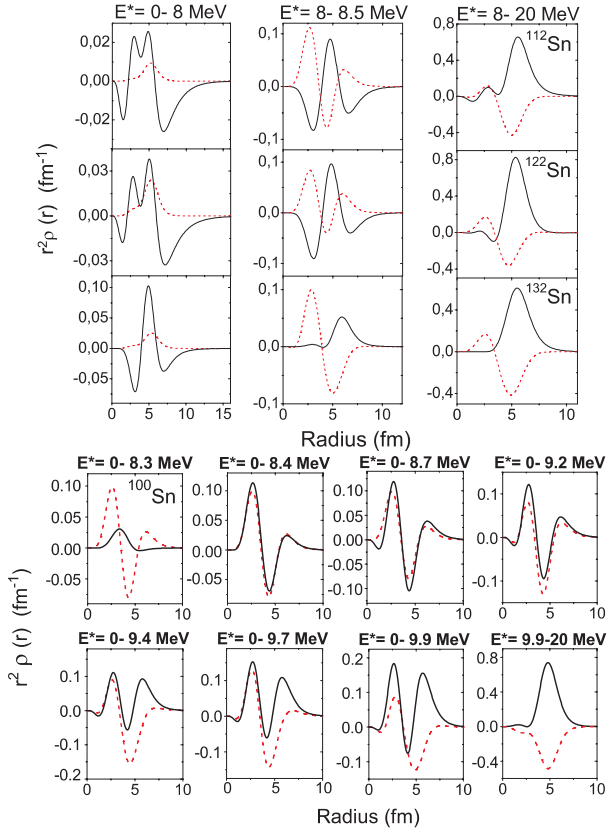

Figure 3. Dipole one-phonon proton and neutron transition densities in Sn isotopes.

For a more detailed insight into the characteristic features of the dipole excitations we consider the evolution of the proton and neutron transition densities in various energy regions. In Figure 3 we display dipole QRPA transition densities for several tin isotopes for three different regions of excitation energies: the low-energy PDR region below the neutron emission threshold, the transitional region up to the GDR and in the GDR region and beyond. The transition densities displayed in Figure 3 were obtained by summing over the transition densities of the individual one-phonon 1^- states located in the energy intervals denoted at the top of each column of the figures. A common features of the presented ^{112,122,132}Sn cases is that up to $E^* = 8$ MeV the protons and neutrons oscillate in phase in the nuclear interior, while at the surface only neutron transitions contribute. This pattern is generic to the lowest dipole states making it meaningful to distinguish these excitations from the well known GDR states. Hence, we are allowed to identify the PDR as a distinct and unique excitation different from the giant dipole resonance (GDR).

The transition of the neutron PDR to a proton PDR manifests itself via the proton and neutron transition densities as well. Thus, in ^{100}Sn the proton oscillations dominate at the nuclear surface due to the formation of a proton skin (see Figure 3 and in Ref. [13]). In comparison, the presence of a neutron skin explains the neutron oscillations at the surface of tin nuclei with A$\leq$106 (see in ref. [13] for more details).

The total PDR strength is found to be closely related to the neutron skin thickness (see Figure 4). The dependence of the calculated total PDR strength ($\sum B(E1)\uparrow$) on the mass number for the whole chain of isotopes $^{100-132}$Sn is shown in Figure 4 and compared to the skin thickness δr, eq. (5) of these nuclides. Here, the sum is taken over QRPA dipole states associated with PDR

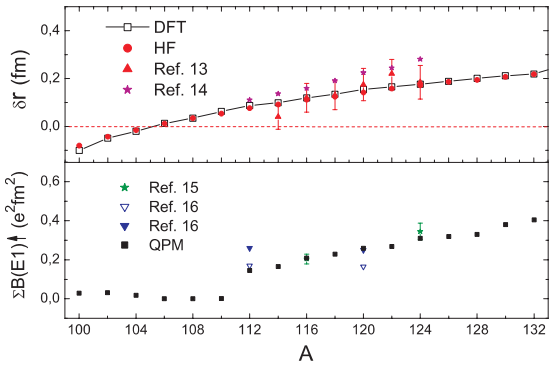

Figure 4. (lower panel) QPM results for the total PDR strengths in the $^{100-132}$Sn isotopes (upper panel) are displayed for comparison together with the nuclear skin thickness δr, eq. (5) (lower panel). Experimental data on the total PDR strengths in ^{116}Sn and ^{124}Sn ref. [23] and ^{112}Sn [24] are also shown. In the lower panel, the skin thickness derived from charge exchange reactions by Krasznahorkay et al. [25, 26] are indicated.

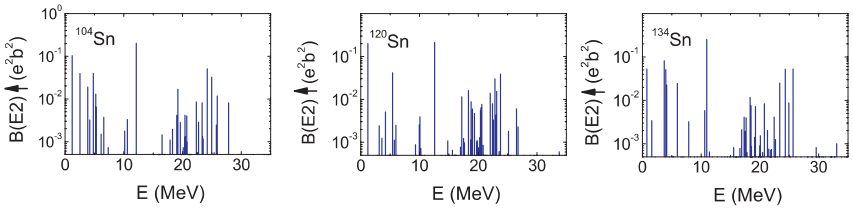

Figure 5. QRPA calculations of electric quadrupole strength distributions in Sn isotopes.

according the analysis of transition densities and the structure of the state's vectors, respectively (see in ref. [13] for more details). The close relationship of the PDR strength and the skin thickness is also confirm in our investigations of $N = 50$, $N = 82$ nuclei [7, 8].

Furthermore, in theoretical investigations of 2^+ excitations in Sn isotopic chain, we find a strength clustering of quadrupole states, at low-energies, with predominantly neutron structure. In the lighter tin isotopes, the reduced neutron number decreases the collectivity of the $[2_1^+]_{QRPA}$ state which becomes non-collective in ^{104}Sn. At the same time, the proton contribution to the B(E2) strength, located in the energy range 2-4 MeV, increases toward ^{104}Sn and brings to more intensive proton quadrupole excitations in ^{104}Sn there. Consequently, the ^{104}Sn nucleus appears to be an opposing case where a change from a neutron to a proton skin occurs. Theoretical results of B(E2) strength distributions

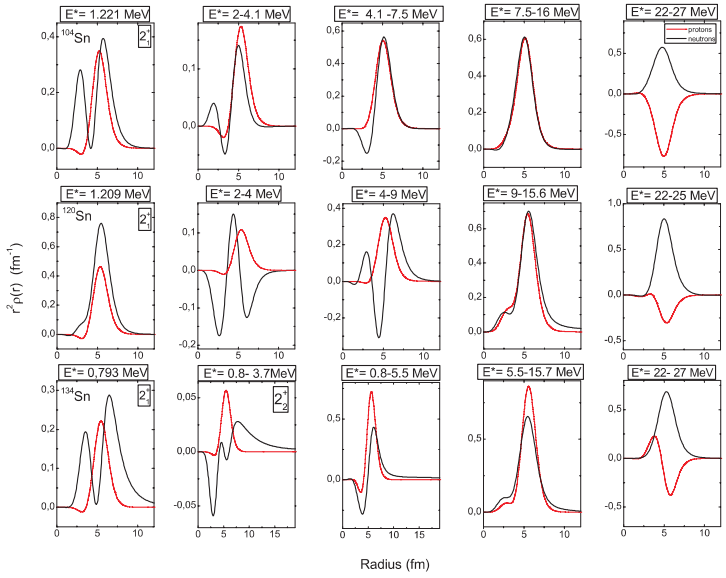

Figure 6. Quadrupole one-phonon proton and neutron transition densities in Sn isotopes.

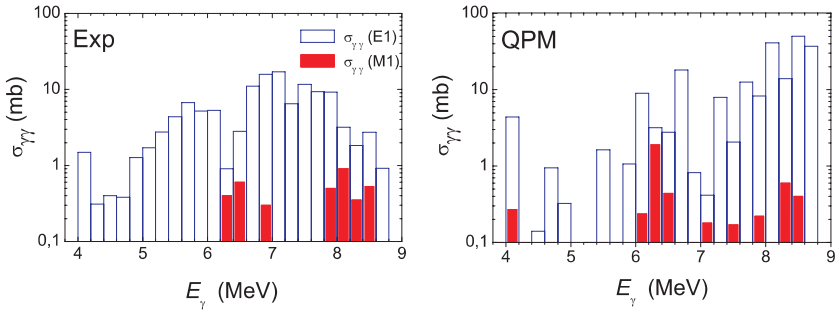

Figure 7. Experimental data (left panel) and QPM calculations (right panel) for $E1$ (electric dipole) and $M1$ (magnetic dipole) photoabsorption cross sections in ^{138}Ba below 9.0 MeV. The cross sections are averaged over 0.2 MeV energy bins (see in Ref.17 as well).

in ^{104,120,134}Sn isotopes are presented in Figure 5. A sizable increase of B(E2) strength at $E_x \approx$ 2-4 MeV is observed for the heaviest tin isotopes - ^{130}Sn and ^{134}Sn - studied in [15, 16]. The clustering of quadrupole states at low-energies shows a pattern similar to the PDR phenomenon. Therefore, we may consider the spectral distribution of a Pygmy Quadrupole Resonance (PQR). Correspondingly, the connection of the PQR with neutron or proton skin oscillations is demonstrated in analysis of transition densities (see in Figure 6). Similarly to the PDR, a transition from a neutron PQR to a proton PQR in ^{104}Sn is observed for the mass region where the neutron skin reverses into a proton skin [15, 16].

An important question to clarify is the fine structure of the observed low-energy dipole strength. For this purpose, QPM calculations of low-energy E1 and spin-flip M1 excitations are made, in a configuration space including up to three-phonon components, in ^{138}Ba nucleus. The results are compared to experimental data obtained from polarized photon beams [14]. The experimental observations and their theoretical interpretation show unambiguously the predominantly electric character of the observed low-energy dipole strength (see Figure 7). Namely, only the electric dipole strength should be related to PDR mode (for more details see in Ref. [14]).

4 Conclusion

The systematic investigations of low-energy dipole excitations in Z=50 isotopic and $N = 50$, 82 isotonic chains reveal PDR- a new dipole mode of a special character. In neutron-rich nuclei, the structure of the PDR is dominated by neutron components while with increase of the proton number, toward $N = Z$, it transforms into a proton one. The PDR transition strength is found directly related to the thickness of a neutron or proton skin. Its generic character is further confirmed by the shape and structure of the related transition densities, showing that this mode is clearly distinguishable from the conventional GDR mode.

In theoretical investigations of low-energy quadrupole states, PQR mode resembling the properties of the PDR is observed. An especially interesting aspect is the close relation of the PQR excitations to the shell structure of the nucleus. The best evidence for this feature is the disappearance of the PQR component in the double magic ^{132}Sn nucleus. Thus, the PQR states contain important information on the structure of the valence shells and their evolution with the nuclear mass number.

In addition, the correlation of the PQR transition strength with the neutron or proton skin thickness manifests itself via a transition from a neutron PQR to a proton PQR in ^{104}Sn, the mass region where the neutron skin reverses into a proton skin.

In $N = 82$ nuclei the low-energy dipole strength is mostly due to electric excitations. Even though, in order to determine the pure PDR strength associated with a nuclear skin, the magnetic contribution must be identified and subtracted.

References

[1] I. Tanihata et al., *Phys. Rev. Lett*. **55** (1985) 2676.
[2] Y. Suzuki *et al*., *Prog. Theor. Phys*. **83** (1990) 180.
[3] P. Van Isacker *et al*., *Phys. Rev. C* **45** (1992) R13.
[4] A. Zilges *et al*., *Phys. Lett*. **B542**, (2002) 43.
[5] T. Aumann, *Eur. Phys. J. A* **26** (2005) 441.
[6] P. Adrich et al., *Phys. Rev. Lett*. **95** (2005) 132501.
[7] S. Volz et al., *Nucl. Phys.* **A779**, (2006) 1.
[8] R. Schwengner et al., *Phys. Rev. C* **78** (2008) 064314.
[9] F. Hofmann and H. Lenske, *Phys. Rev. C* **57** (1998) 2281.
[10] V.G. Soloviev, *Theory of complex nuclei* (Oxford: Pergamon Press, 1976).
[11] N. Tsoneva, H. Lenske, Ch. Stoyanov, *Phys. Lett.* **B586** (2004) 213.
[12] N. Paar et al., *Rep. Prog. Phys*. **70** (2007) 691 and refs therein.
[13] N. Tsoneva, H. Lenske, *Phys. Rev. C* **77** (2008) 024321 and refs. therein.
[14] A. Tonchev et al., *Phys. Rev. Lett*. **104** (2010) 072501.
[15] N. Tsoneva, H. Lenske, *Mod. Phys. Lett*. **A** (2010) 1779.
[16] N. Tsoneva, H. Lenske, *Phys. Lett. B* in press, doi:10.1016/j.physletb.2010.11.002.
[17] A. Vdovin, V.G. Soloviev, *Physics of Elementary Particles and Atomic Nuclei* **14** (1983) 237.
[18] P. Hohenberg, W. Kohn, *Phys. Rev. B* **136** (1964) 864.
[19] W. Kohn, L.J. Sham, *Phys. Rev. A* **140** (1965) 1133.
[20] G. Audi, A.H. Wapstra, *Nucl. Phys*. **A595** 409 (1995).
[21] M. Grinberg, Ch. Stoyanov, *Nucl. Phys*. **A573** (1994) 231.
[22] V.Yu. Ponomarev, Ch. Stoyanov, N. Tsoneva, et al., *Nucl. Phys*. **A635** (1998) 470.
[23] K. Govaert et al., *Phys. Rev. C* **57** (1998) 2229.
[24] B. Özel et al., arXiv:0901.2443.
[25] A. Krasznahorkay et al., *Phys. Rev. Lett*. **82** (1999) 3216.
[26] A. Krasznahorkay et al., *AIP* **610** (2002) 751.